JACS
JOURNAL OF THE AMERICAN CHEMICAL SOCIETY
Article
pubs.acs.org/JACS

Facile Synthesis of $Ba_{1-x}K_xFe_2As_2$ Superconductors via Hydride Route

Julia V. Zaikina,*[,†,‡] Maria Batuk,[§] Artem M. Abakumov,[§] Alexandra Navrotsky,[‡] and Susan M. Kauzlarich*[,†]

[†]Department of Chemistry and [‡]Peter A. Rock Thermochemistry Laboratory and NEAT ORU, University of California at Davis, One Shields Avenue, Davis, California 95616, United States

[§]EMAT, University of Antwerp, Groenenborgerlaan 171, B-2020 Antwerp, Belgium

Supporting Information

ABSTRACT: We have developed a fast, easy, and scalable synthesis method for $Ba_{1-x}K_xFe_2As_2$ ($0 \leq x \leq 1$) superconductors using hydrides BaH_2 and KH as a source of barium and potassium metals. Synthesis from hydrides provides better mixing and easier handling of the starting materials, consequently leading to faster reactions and/or lower synthesis temperatures. The reducing atmosphere provided by the evolved hydrogen facilitates preparation of oxygen-free powders. By a combination of methods we have shown that $Ba_{1-x}K_xFe_2As_2$ obtained via hydride route has the same characteristics as when it is prepared by traditional solid-state synthesis. Refinement from synchrotron powder X-ray diffraction data confirms a linear dependence of unit cell parameters upon K content as well as the tetragonal to orthorhombic transition at low temperatures for compositions with $x < 0.2$. Magnetic measurements revealed dome-like dependence of superconducting transition temperature T_c upon K content with a maximum of 38 K for x close to 0.4. Electron diffraction and high-resolution high-angle annular dark-field scanning transmission electron microscopy indicates an absence of Ba/K ordering, while local inhomogeneity in the Ba/K distribution takes place at a scale of several angstroms along [110] crystallographic direction.

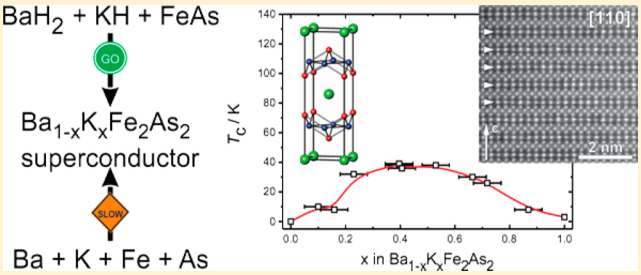

INTRODUCTION

Interest in iron arsenide superconductors has been growing[1] since the discovery of superconductivity at 26 K in the oxopnictide $LaFeAsO_{1-x}F_x$[2] in 2008. Subsequently other parent compounds have been identified, including AFe_2As_2 (A = Ca, Ba, Sr, Eu), AFeAs (A= Li or Na), FeE (E = Se or Se/S/Te), where doping or application of external pressure induces superconductivity.[3] Superconductivity in the $BaFe_2As_2$[4] parent compound (Figure 1) can be realized either by hole doping through partial substitution of Ba^{2+} by Na^+, K^+ or Rb^+ [5−8] or by electron doping via partial substitution of Fe by Co or Ni[9] or even by isovalent substitutions of As by P.[10] The most studied and well characterized system is the superconducting solid solution $Ba_{1-x}K_xFe_2As_2$, where a maximum T_c of 38 K is observed for x close to 0.4.[7,11]

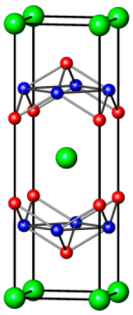

Figure 1. Crystal structure of $BaFe_2As_2$. Ba: green, Fe: blue, As: red.

Compared to cuprates, Fe-based superconductors have several advantages for practical applications,[12−14] such as low anisotropy and large upper critical field H_{c2} up to 250 T. Since their critical temperature T_c is higher than that of niobium-based superconductors, Fe-based superconductors are an attractive replacement for magnet applications at 20−50 K temperature range.[14] For practical applications such as magnets and cables, the powder-in-tube (PIT) technique has been suggested,[14] which includes packing of the corresponding powdered materials into a metal tube, that is further swaged and drawn to wire with a heat treatment if necessary. The method proposed to fabricate iron-based superconducting wires via the PIT technique can be realized *in situ* or *ex situ*. For *in situ* PIT, the mixture of starting materials is packed into a metal tube, and the annealing is performed after wire shaping, while in the *ex situ* PIT method, the presynthesized superconducting materials are packed into metal tubes.[14] While convenience of the *in situ* PIT method is evident, the wires obtained by heat treatment of the elements have low critical current density due to the current blocking associated with cracks, porosity, grain boundary wetting by secondary phases, and phase inhomogeneities.[13,14] Slow kinetics of the processes associated with the

Received: September 25, 2014
Published: November 11, 2014

dx.doi.org/10.1021/ja509907r | J. Am. Chem. Soc. 2014, 136, 16932−16939

preparation of K-doped $BaFe_2As_2$ and related compounds by heat treatment of the elements is a reason for the observed poor material behavior. The presence of secondary current blocking phases as well as oxygen-rich amorphous layers may alter the intergranular connectivity and thus impair material performance.[14] Therefore, a fast route which gives access to fine and homogeneous powders of doped $BaFe_2As_2$ superconductors is highly desirable.

Despite very active research in the field of iron arsenide superconductors, the synthesis of the K-doped $BaFe_2As_2$ still remains a challenge. The associated synthetic difficulties include high vapor pressure and toxicity of arsenic, high moisture/oxygen affinity, and low melting points and volatility of potassium and barium. The solid-state method used for the preparation of K-doped $BaFe_2As_2$ from the elements includes several annealing steps with intermediate regrinding and pressing of the pellets needed to improve homogeneity of the products and facilitate diffusion of the components.[11,15] Another suggested method for the preparation of the bulk microcrystalline K-doped $BaFe_2As_2$ includes reaction of the presynthesized precursors, such as BaAs, K_3As, and Fe_2As at 1323 K.[16]

We have developed a new synthesis method utilizing potassium and barium hydrides as reactive precursors to prepare K-doped $BaFe_2As_2$. The hydride route to nonoxide materials has been explored for Zintl phases, such as Na_4Si_4, Na_4Ge_4, K_4Ge_4, Mg_2Si.[17,18] Synthesis from hydrides provides better mixing and easy handling of the starting materials (unlike elemental K and Ba, corresponding hydrides are salt-like powders), consequently leading to lower synthesis temperatures and/or faster reactions. Another important feature of the hydride route is the reducing atmosphere provided by the evolved hydrogen, thus facilitating preparation of oxygen-free powders. The hydride route is also expected to facilitate sintering and preparation of dense samples, since the powders feature clean, oxygen-free surfaces. Several experimental parameters can be varied to optimize synthesis conditions, e.g., stoichiometry, temperature, time, and ball milling vs hand grinding.[17] We show by synchrotron X-ray powder diffraction, magnetometry, and transmission electron microscopy that the samples of $Ba_{1-x}K_xFe_2As_2$ prepared by the new hydride route exhibit identical structural parameters and similar dependence of T_c upon the K content as samples prepared by the traditional solid-state method.

EXPERIMENTAL SECTION

Chemicals. Barium hydride powder (BaH_2, Materion Advanced Chemicals, 95%), iron powder (Fe, Puratronic, 99.999%, 22 mesh), and arsenic pieces (As, Johnson Matthey, 99.9999%) were used as received. Potassium hydride (KH, 30 wt % dispersion in mineral oil, Sigma-Aldrich) was washed with hexane several times and dried in vacuum before use. All manipulations were carried out in a glovebox under dry argon atmosphere. Iron arsenide FeAs precursor was synthesized by reaction of stoichiometric mixtures of iron powder and arsenic powder prepared from pieces by grinding in an agate mortar. A silica glass ampule with iron and arsenic mixtures in 1:1 molar ratio were sealed under vacuum and slowly heated to 873 K in 10 h and annealed at this temperature for 24 h, then heated to 1273 K in 12 h and annealed at this temperature for 24 h and furnace cooled. According to powder X-ray diffraction (PXRD), the FeAs precursor contains up to 6 wt % of $FeAs_2$ impurity.

Caution: Barium hydride and potassium hydride powders are reactive to oxygen and moisture and must be handled under an inert atmosphere with care.

Sample Preparation. Samples of $Ba_{1-x}K_xFe_2As_2$ ($0 \le x \le 1$) were prepared according to the following general procedure, which includes ball milling of BaH_2 and/or KH hydrides together with premade FeAs precursor or elemental Fe and As in the different stoichiometric ratios followed by annealing at different temperatures for 48 h in sealed Nb containers. A high-energy Spex 8000 M mill with a tungsten carbide lined grinding vial set (volume 5 mL) and one tungsten carbide ball (diameter 1.12 cm) was used to ball mill mixtures of BaH_2 and/or KH with FeAs precursor or with elemental Fe and As in a desired molar ratio with a total mass of 0.5 g. The milling vial was additionally sealed in a metal-coated plastic bag in a glovebox under argon atmosphere to prevent oxidation of the components during ball milling. The reagents were intimately mixed in the mill for 30 min, and the milling vial was returned to the glovebox for further manipulation. The ball milled powders (total mass ~0.5 g) were loaded into Nb containers (typical size: length ~6 cm, ID 7.6 mm, OD 9.4 mm) sealed from one end with an arc welder. The filled Nb containers were subsequently sealed under reduced Ar pressure with an arc welder and further sealed under vacuum in evacuated silica tubes (ID 16 mm, OD 18 mm, length ~200 mm, pressure 20 mTorr). The tubes were heated to different temperatures (773, 973, 1073, 1173 K) with a heating rate of ~1.1 K/min, annealed for 48 h at the desired temperature, and furnace cooled to room temperature. The Nb containers were opened in a glovebox. Samples were stored in a glovebox to prevent oxidation. To prevent possible overpressure of the sealed evacuated silica ampule due to the evolved gas products, two different setups were used. One was to place the sealed Nb container in the middle of the silica tube with stopcocks at both ends. The silica tube was placed into a horizontal furnace, connected to the flowing Ar stream (flow rate 30 mL/min), and heated to the desired temperature. To compensate heat uptake by flowing argon, higher annealing temperatures were used (e.g., in order to obtain the desired 1173 K; the temperature was set to 1273 K). Alternatively, the silica tube was fitted with a pressure relief check valve and a valve to evacuate the tube and then close during the annealing (Figure S1).

Additional experiments were conducted to evaluate the possible mechanism of the reaction of hydrides with iron arsenide. The premilled mixtures of BaH_2:FeAs = 1.1:2 molar ratio were loaded into a 1 mL alumina boat with an inverted alumina boat (1.5 mL) serving as a lid and placed into a silica tube with stopcocks at both ends. The silica tube was placed into a horizontal furnace, connected to the flowing Ar stream (flow rate 30 mL/min), and heated to 973 K with heating rate of 2.8 K/min and held at this temperature for 24 h. To detect any arsine (AsH_3) gas that might be a potential side product, the argon gas was bubbled through a saturated (concentrated) solution of silver nitrate $AgNO_3$ (Gutzeit test). The color change of the solution from colorless to black indicates presence of evolved arsine according to the equation:

$$AsH_3 + 3AgNO_3 \rightarrow Ag_3As \downarrow + 3HNO_3$$

Caution: The reaction of hydrides with arsenic may under some circumstances result in the formation of acutely toxic and flammable arsine gas AsH_3. Appropriate precautions should be taken in the performance of the reactions described.

Characterization. Samples were analyzed by powder X-ray diffraction (PXRD) on a Bruker D8 Advance X-ray diffractometer in Bragg–Brentano geometry with Cu Kα radiation (λ = 1.54178 Å). Data were collected on a zero-background plate holder in air. For selected samples high-resolution synchrotron powder diffraction data were collected using beamline 11-BM at the Advanced Photon Source (APS), Argonne National Laboratory with an average wavelength of 0.413830 Å. Discrete detectors covering an angular range from −6 to 16° 2θ were scanned over a 34° 2θ range, with data points collected every 0.001° 2θ with a scan speed of 0.01°/s. Samples of $Ba_{1-x}K_xFe_2As_2$ were mixed with amorphous silica to achieve reasonable transmission and packed in capillaries, which were glued inside an argon filled glovebox. Data were collected at room temperature and additionally at 100 K for samples with x = 0 and 0.2. Diffraction patterns were analyzed by the Rietveld refinement method using the Jana2000 software package.[19] For each sample the

profile parameters, background parameters, zero correction, and lattice constants were refined first. The background was fitted using a shifted 14- or higher-order Chebyshev polynomial function. A pseudo-Voigt function was applied to generate the profile shape. For the $Ba_{1-x}K_xFe_2As_2$ phase, atomic coordinates and occupancy factors, in particular Ba/K ratios and *z*-coordinate for the As position, were refined. The preferential orientation of crystallites was taken into account. The results of the Rietveld refinement are listed in Table S1. To get realistic estimated standard deviations (esd's) for Ba/K occupancies and unit cell parameters, Berar's factor was applied.[20]

Magnetic susceptibility was measured on a cold-pelletized microcrystalline sample (mass 20−60 mg) with a Quantum Design SQUID magnetometer MPMS-XL. DC magnetic susceptibility measurements were carried out in an applied field of 10 Oe in the 2−200 K range. The sample was cooled without an external magnetic field applied, and then susceptibility was measured at the external field of 10 Oe on heating to 200 K (ZFC, zero-field cooled) and on cooling down to 2K (FC, field cooled).

Samples for the TEM study were prepared in the Ar-filled glovebox by grinding the material under hexane and depositing a few drops of the suspension onto holey carbon grids. The samples were transported into the microscope column completely avoiding contact with air. The samples were investigated using electron diffraction (ED) and high-resolution high-angle annular dark-field scanning transmission electron microscopy (HAADF-STEM). The ED patterns were recorded on an FEI Tecnai G2 electron microscope operated at 200 kV. The HAADF-STEM images were collected on a probe aberration-corrected microscope FEI Titian 50−80 operated at 200 kV.

RESULTS AND DISCUSSION

Synthesis and Characterization of $BaFe_2As_2$ and KFe_2As_2 Parent Compounds. The experimental parameters, such as temperature and hydrides/FeAs ratio, were varied in order to optimize the preparation of single phase samples of $BaFe_2As_2$ and KFe_2As_2, while the duration of annealing was kept the same for all synthesis temperatures (48 h). It was determined that ball milling is crucial for the preparation of single phase samples since it provides uniform mixing of initial reagents and it was used in all syntheses. Synthesis of samples $BaFe_2As_2$ and KFe_2As_2 was performed by reacting either elemental Fe and As or presynthesized FeAs with corresponding hydrides BaH_2 or KH.

Synthesis of $BaFe_2As_2$ was attempted at three different temperatures: 773, 973, 1173 K starting from BaH_2 and FeAs. A single phase sample was obtained at 1173 K, while synthesis at lower temperatures led to incomplete reaction and significant leftovers of unreacted FeAs (Table S2). Occasionally, a small excess of BaH_2, e.g., BaH_2/FeAs = 1.1/2 was used, since commercially available BaH_2 has 95% purity. When synthesized from elemental iron and arsenic, a larger excess of BaH_2 is required. The optimized conditions are summarized in Table 1.

$BaFe_2As_2$ undergoes a spin density wave transition at low temperatures (T_{SDW} = 140 K) accompanied by a structural distortion from *I*-tetragonal cell to *F*-orthorhombic ($a_{orthorhombic} \approx \sqrt{2}a_{tetragonal}$; $c_{orthorhombic} \approx c_{tetragonal}$).[4] To verify the presence of this structural transition for $BaFe_2As_2$ obtained via hydride route, synchrotron PXRD data were collected at room temperature and at 100 K (Table S1, Figure S2).

The splitting of several reflections, for instance (110) and (112) upon cooling down to 100 K indicates the *I*-tetragonal cell to *F*-orthorhombic structural distortion (Figure 2, top) similar to that reported for $BaFe_2As_2$ prepared from elements.[4]

Optimization of synthesis conditions was performed for KFe_2As_2 starting from KH and FeAs (Table S2). Synthesis at 1173 K results in the presence of Fe_2As and K_3As impurities,

Table 1. Optimized Conditions for Synthesis of $Ba_{1-x}K_xFe_2As_2$ ($0 \le x \le 1$)[a]

refined composition,[d] nominal *x*	molar ratios	annealing temperature (K)[b]	impurity (wt %)
$BaFe_2As_2$	BaH_2/FeAs = 1/2 or 1.1/2	1173	–
$BaFe_2As_2$	BaH_2/Fe/As = 1.2/2/2	1173	–
KFe_2As_2	KH/FeAs = 1.3/2	973	–
KFe_2As_2	KH/FeAs = 1.3/2	773[c]	–
KFe_2As_2	KH/Fe/As = 1.3/2/2	973	–
$Ba_{1.1(1-x)}K_{1.3x}Fe_2As_2$ (FeAs as precursor)			
$Ba_{0.13}K_{0.87(5)}Fe_2As_2$ *x* = 0.9	BaH_2/KH/FeAs = 0.11/1.17/2	973	–
$Ba_{0.32}K_{0.68(6)}Fe_2As_2$ *x* = 0.7	BaH_2/KH/FeAs = 0.33/0.91/2	973	–
$Ba_{0.46}K_{0.54(4)}Fe_2As_2$ *x* = 0.5	BaH_2/KH/FeAs = 0.55/0.65/2	973	–
$Ba_{0.61}K_{0.39(3)}Fe_2As_2$ *x* = 0.4	BaH_2/KH/FeAs = 0.66/0.52/2	1073	–
$Ba_{0.84}K_{0.16(3)}Fe_2As_2$ *x* = 0.2	BaH_2/KH/FeAs = 0.88/0.26/2	1073	FeAs (2)
$Ba_{1.1(1-x)}K_{1.3x}Fe_2As_2$ (elemental Fe and As as precursors)			
$Ba_{0.35}K_{0.65(5)}Fe_2As_2$ *x* = 0.7	BaH_2/KH/Fe/As = 0.33/0.91/2/ 2	973	Fe_2As (3)
$Ba_{0.48}K_{0.52(6)}Fe_2As_2$ *x* = 0.5	BaH_2/KH/Fe/As = 0.55/0.65/2/ 2	973	Fe_2As (6)
$Ba_{0.78}K_{0.22(4)}Fe_2As_2$ *x* = 0.3	BaH_2/KH/Fe/As = 0.77/0.39/2/ 2	1073	Fe_2As (5)

[a]Note that excess of hydrides was used. [b]Starting materials were ball milled for 30 min and annealed for 2 days (see Experimental Section for details). [c]Sample prepared at 773 K exhibits lower crystallinity resulting in broader XRD peaks and slight variation in unit cell parameters. [d]Composition determined by Rietveld refinement (see Table S1 and Experimental Section).

suggesting that the annealing at 1173 K leads to the partial decomposition of KFe_2As_2, and therefore this temperature is too high. It was determined that an excess of KH is needed, since synthesis with KH:FeAs ratio of 1:2 leads to the presence of residual FeAs. The synthesis temperature was lowered to 973 K, and excess KH was used. The optimized conditions for synthesis of KFe_2As_2 phase can be summarized as follows: KH:FeAs in the ratio of 1.3:2, ball milled for 30 min, and annealed at 973 K for 48 h. A single phase sample of KFe_2As_2 can be obtained at temperatures as low as 773 K (Table 1), but the product exhibits lower crystallinity resulting in broader PXRD peaks and slight variation in unit cell parameters (Figure S3).

For the ternary KFe_2As_2 prepared via the hydride route, we observe variation in the unit cell parameters beyond their uncertainties, suggesting a homogeneity range for this phase. Refinement of atomic occupancies results in only slight deviation from unity for the K (s.o.f. 98 ± 1%) or Fe (s.o.f. 92 ± 6%) atomic sites. The single phase sample of KFe_2As_2 can be synthesized not only from the FeAs precursor but also from elemental Fe and As with addition of excess of KH at 973 K (Table 1). KFe_2As_2 prepared via the hydride route is air and moisture sensitive similar to KFe_2As_2 prepared from elements.[21] When left in air, it decomposes into $KAsO_3$ and hydrated Fe_2O_3.

An excess of hydrides (BaH_2 or KH) is necessary to produce single phase samples in case of KFe_2As_2 and $BaFe_2As_2$. This can be attributed to several reasons: the commercially available hydrides have 95−97% purity and thus may contain small

dx.doi.org/10.1021/ja509907r | J. Am. Chem. Soc. 2014, 136, 16932−16939

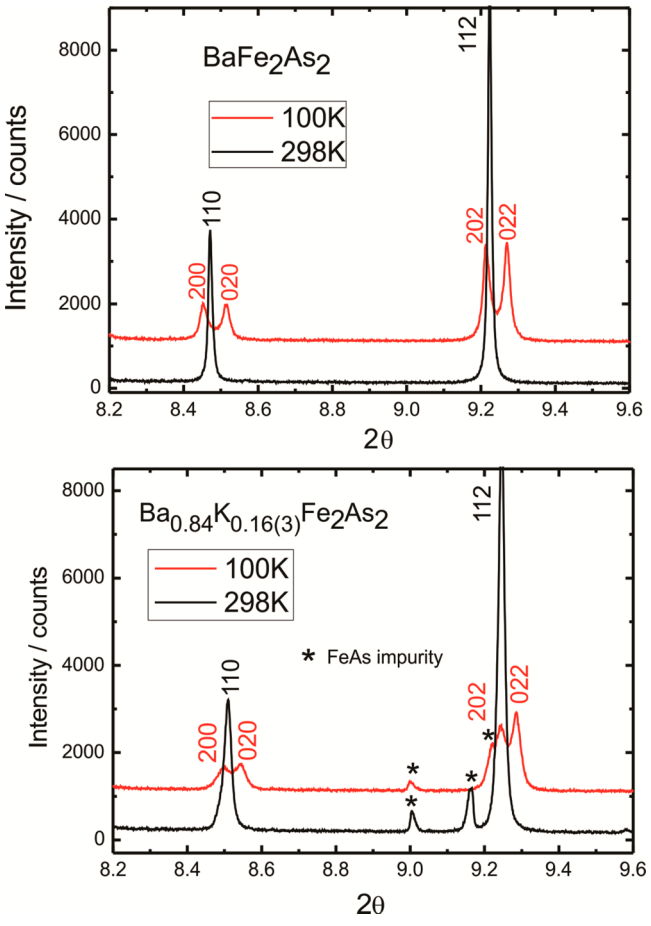

Figure 2. Splitting of (110) and (112) reflections for $BaFe_2As_2$ (top) and $Ba_{0.84}K_{0.16(3)}Fe_2As_2$ (bottom) upon cooling from room temperature (black) to 100 K (red).

amounts of oxidation products. Additionally, due to its volatility, excessive potassium may be deposited on the walls of the niobium crucible. Notably, excess of the corresponding metals (Ba) was used for synthesis of $BaFe_2As_2$ from the elements.[4] Additionally, significant excess of hydrides is required for the preparation of Zintl phases, Na_4Si_4, Na_4Ge_4, and K_4Ge_4 from Si or Ge and corresponding NaH and KH hydrides.[17]

Synthesis and Characterization of $Ba_{1-x}K_xFe_2As_2$. Once the synthesis of the ternary $BaFe_2As_2$ and KFe_2As_2 was optimized, the solid solution $Ba_{1-x}K_xFe_2As_2$ was prepared following a similar procedure. An excess of KH and BaH_2 was used, leading to the nominal composition $Ba_{1.1(1-x)}K_{1.3x}Fe_2As_2$. The annealing temperature was initially chosen as 973 K, however for K-poor compositions ($x \leq 0.4$), synthesis at 973 K resulted in the presence of residual FeAs, while annealing at 1073 K led to nearly single phase product. Similarly to the parent ternary compounds, the synthesis of $Ba_{1-x}K_xFe_2As_2$ from elements requires an excess of the corresponding hydrides (Table 1).

The formation of $Ba_{1-x}K_xFe_2As_2$ from hydrides and FeAs can be described by the following equation:

$$(1-x)BaH_2 + xKH + 2FeAs \rightarrow Ba_{1-x}K_xFe_2As_2 + (1-x/2)H_2\uparrow$$

which implies that hydrogen gas is evolved during synthesis. According to the Gutzeit test, which is used to detect arsenic in the form of arsine AsH_3, no arsine is evolved during heat treatment of BaH_2 and FeAs. Nb is known to be permeable to hydrogen, and Nb-based alloys have been suggested to use for hydrogen permeable membranes.[22−24] Starting components were annealed in a sealed Nb tube encapsulated in a evacuated silica tube. Since hydrogen is being evolved during the reaction, leading to the buildup of the pressure in the silica tube, larger amounts (>0.5 g) of the starting materials can be annealed under flow of argon gas or with a pressure relief valve (Figure S1).

Refinement of the Ba/K ratio in $Ba_{1-x}K_xFe_2As_2$ samples using laboratory or synchrotron PXRD data revealed that the nominal composition is close to the actual one obtained from the refinement (Tables 1 and S1). The dependence of the tetragonal unit cell parameters, *a* and *c*, upon K content, *x*, is linear in accordance with Vegard's law with *a* parameter decreasing, and *c* parameter increasing with increase of K content (Figure 3). Considering the error bars, the unit cell parameters for $Ba_{1-x}K_xFe_2As_2$ prepared via hydride route are identical to those for $Ba_{1-x}K_xFe_2As_2$ prepared by standard solid-state techniques from elements.[7]

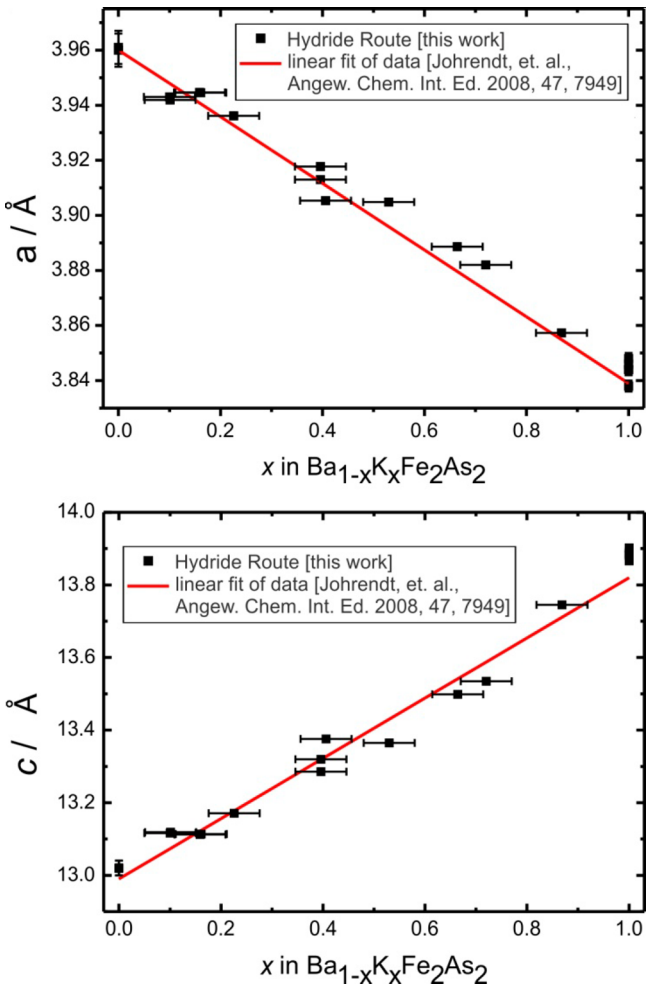

Figure 3. Variation of unit cell parameters with potassium content, *x*, in $Ba_{1-x}K_xFe_2As_2$. For comparison linear fit of data by Johrendt et al.[7] is plotted as red line. Error bars for the unit cell parameters are smaller than the symbols used for the experimental data.

dx.doi.org/10.1021/ja509907r | J. Am. Chem. Soc. 2014, 136, 16932−16939

Doping with potassium is known to suppress the spin density wave transition and structural distortion from *I*-tetragonal to *F*-orthorhombic cell and induces superconductivity at low temperatures.[7,11] However, for low potassium concentrations ($x \leq 0.2$) a structural transition from tetragonal to orthorhombic phase still takes place.[7] Synchrotron PXRD data collected at room temperature and at 100 K (Table S1, Figure S2) for a $Ba_{0.84}K_{0.16(3)}Fe_2As_2$ sample prepared via hydride route indicate the splitting of (110) and (112) reflections upon cooling to 100 K (Figure 2, bottom). This is consistent with *I*-tetragonal to *F*-orthorhombic structural distortion similar to that reported for $Ba_{0.8}K_{0.2}Fe_2As_2$ prepared from elements.[7]

Alkaline-earth and rare-earth metal hydrides, CaH_2, LaH_2, CeH_2, and SmH_2 have been used for the high-pressure synthesis of other representatives of the iron arsenide superconductors family, $LnFeAsF_{1-x}H_x$ (x = 0.0−1.0; Ln = Ca or La) and $LnFeAsO_{1-x}H_x$ (Ln = Ca, La, Ce, Sm).[25−27] For this preparation, high pressures (~2 GPa) and high temperatures (up to 1473 K) as well as a supplementary hydrogen source ($LiBH_4$ or $NaBH_4$) are required to force H^- ions to occupy F^- sites between FeAs layers. In the case of $LnFeAsO_{1-x}H_x$ (Ln = Ca, La, Ce, Sm) the hydrogen substitution as H^- into the O^{2-} site provides excess electrons to the FeAs layer, giving rise to superconductivity with a maximum T_c of 56 K for $SmFeAsO_{0.75}H_{0.25}$. Incorporation of hydrogen into SmFeAsO leads to substantial contraction of the unit cell volume and subsequent change of the electronic properties due to hydrogen doping, which results in a concomitant change in T_c. We do not see any variation of unit cell parameters for $Ba_{1-x}K_xFe_2As_2$ prepared by the hydride route. To further confirm the absence of hydrogen doping, samples of $Ba_{1-x}K_xFe_2As_2$ have been analyzed by magnetometry.

Magnetic Properties. $BaFe_2As_2$ prepared via hydride route exhibits weak, slightly temperature-dependent paramagnetism with a small magnetic anomaly at around 140 K, which is associated with spin-density wave transition (Figure S4a). This is consistent with the literature data on powdered sample of $BaFe_2As_2$ made from elements.[4] The powdered sample of KFe_2As_2 shows the sharp onset of superconducting transition for both ZFC and FC curves at T_c = 3.5 K (Figure S4b); the superconducting transition temperature is concordant with the literature data.[28−31]

Bulk superconductivity in the samples of $Ba_{1-x}K_xFe_2As_2$ was observed for all the compositions with $x > 0.2$, as is evident from the temperature dependence of magnetic susceptibility (Figure 4, insert). Superconducting transitions are sharp for samples with doping level close to optimum, $x \approx 0.4$, while for x close to 0.2 and 0.7, transitions are somewhat broader. The superconducting volume fractions correspond to 65% for the optimal K concentration. The superconducting transition temperature, T_c, has been calculated from the onset of superconducting transitions and has a strong dependence on K content, reaching a maximum of 38 K for x close to 0.4. The dependence of T_c has characteristic dome-like dependence upon K content analogous to that for $Ba_{1-x}K_xFe_2As_2$ prepared from elements.[7]

Transmission Electron Microscopy. The variation of the K concentration is believed to be one of the crucial factors governing the observed electronic inhomogenties and phase separations into magnetically ordered and superconducting phases.[32−36] Potassium dopant clustering and nanoscale

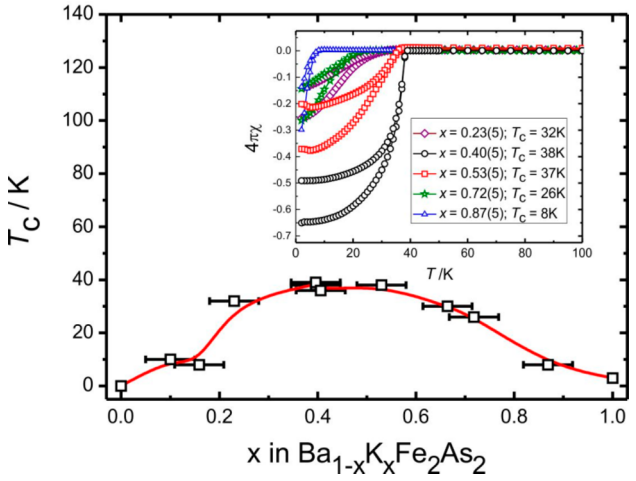

Figure 4. Compositional dependence of superconducting transition temperature, T_c, upon potassium content, x, in $Ba_{1-x}K_xFe_2As_2$. Insert: temperature dependence of magnetization measured in the applied field of 10 Oe.

inhomogenties have been detected by atom probe tomography[37] on the surfaces of $Ba_{0.72}K_{0.28}Fe_2As_2$ crystals obtained from FeAs flux and $Sr_{0.75}K_{0.25}Fe_2As_2$ crystals by scanning tunneling microscopy.[34] Since hydrides provide better mixing, the distribution of the K-dopant is expected to be more homogeneous. To study the Ba/K distribution, samples of $Ba_{0.5}K_{0.5}Fe_2As_2$ and $Ba_{0.6}K_{0.4}Fe_2As_2$ were analyzed by means of ED and HAADF-STEM. To the best of our knowledge, this is the first example of detailed investigation of $Ba_{1-x}K_xFe_2As_2$ by HAADF-STEM.

Typical ED patterns taken along the [001], [100], and [110] crystallographic axes of the structure for the sample $Ba_{0.5}K_{0.5}Fe_2As_2$ (Figure 5) can be consistently indexed in a

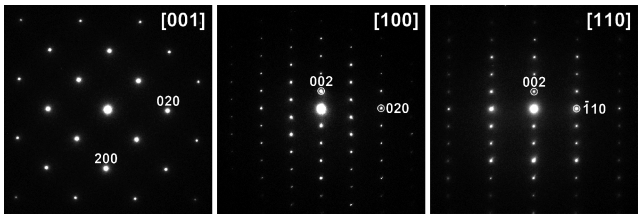

Figure 5. ED patterns along the main crystallographic axes of the $Ba_{0.5}K_{0.5}Fe_2As_2$ structure.

tetragonal lattice with the cell parameters $a \sim 3.8$ Å, $c \sim 13.1$ Å, and $I4/mmm$ space group, which agrees with PXRD data. The ED patterns for the $Ba_{0.6}K_{0.4}Fe_2As_2$ sample look the same and are given in Figure S5.

HAADF-STEM images for $Ba_{0.5}K_{0.5}Fe_2As_2$ taken along the [001], [100], and [110] directions are shown in Figure 6. In this microscopy technique the intensity scales approximately as $I \sim Z^2$, where Z is an average atomic number of the projected column. HAADF-STEM images can provide the information on the distribution of atomic species in the structure (Z_{Ba} = 56, Z_K = 19, Z_{Fe} = 26, Z_{As} = 33). Images taken along the [001] and [100] zone axes do not indicate any Ba/K ordering, and therefore their distribution is completely homogeneous being viewed along these directions. The HAADF-STEM image along the [110] zone axis demonstrates differences in the intensity of the dots attributed to the Ba/K columns (Ba/K layers are

dx.doi.org/10.1021/ja509907r | J. Am. Chem. Soc. 2014, 136, 16932−16939

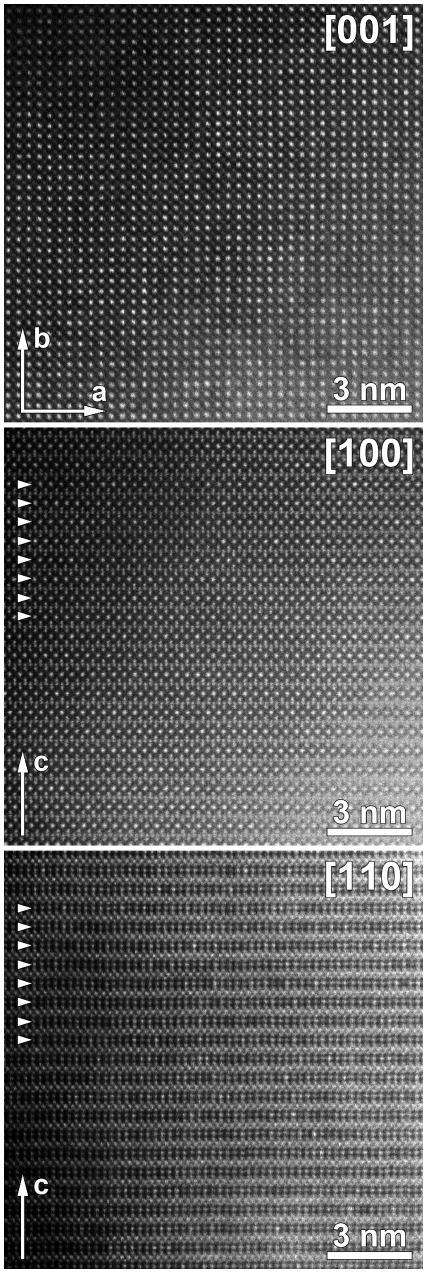

Figure 6. HAADF-STEM images for the $Ba_{0.5}K_{0.5}Fe_2As_2$ sample taken along [001], [100], and [110] zone axes. Arrowheads indicate the Ba/K layers in the structure. The structure looks homogeneous along [001] and [100] directions, while along the [110] direction some Ba/K columns appear noticeably brighter or weaker than the others, indicating slightly inhomogeneous Ba/K distribution.

pointed with arrowheads). Using the HAADF-STEM images, we measured the intensities associated with the columns corresponding to Ba/K and Fe. The intensity distribution is plotted in Figure S6. The intensity spread of the Fe columns can be attributed to the variable thickness of the crystal. One can expect the same intensity spread for the Ba/K columns for the completely homogeneous Ba/K distribution, but the observed intensity variation of the Ba/K columns is noticeably broader, indicating that some columns are Ba-enriched, whereas some are Ba-depleted. However, in general the occurrence of such columns seems to be random in the structure.

In the enlarged [110] HAADF-STEM image in Figure 7, only two areas (marked with brackets) demonstrate ordered

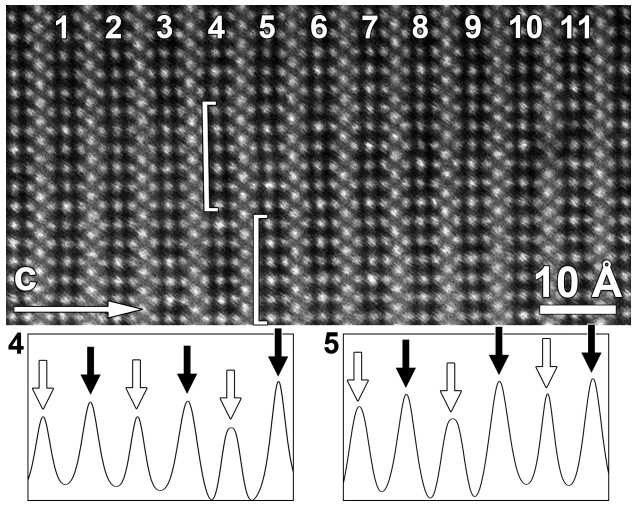

Figure 7. Enlarged [110] HAADF-STEM image for the $Ba_{0.5}K_{0.5}Fe_2As_2$ sample with marked Ba/K layers 1–11. The intensity profiles were measured from the parts marked with brackets in layers 4 and 5. Alternation of the Ba-enriched and Ba-depleted columns is marked with black and white arrows, respectively. No specific ordering occurs for the rest of the layers.

alternation between Ba-depleted (indicated with white arrows at the intensity profiles) and Ba-enriched columns (indicated with black arrows). Such alternation would lead to a $\sqrt{2}a \times \sqrt{2}a \times c$ superstructure, with the [001] projection shown in Figure 8. The complete set of the profiles measured for the Ba/

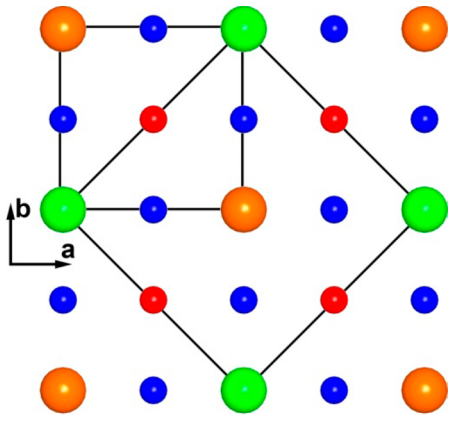

Figure 8. Scheme of the Ba/K ordering in $Ba_{0.5}K_{0.5}Fe_2As_2$ viewed along the [001] direction. The unit cells of the basic $a \times a \times c$ structure and of the $\sqrt{2}a \times \sqrt{2}a \times c$ superstructure are outlined. Ba: green, K: orange, Fe: blue, As: red.

K layers are shown in Figure S7. No pronounced Ba/K ordering was observed on the HAADF-STEM images taken for the $Ba_{0.6}K_{0.4}Fe_2As_2$ sample (Figures S8 and S9).

ED and HAADF-STEM study of $Ba_{0.5}K_{0.5}Fe_2As_2$ and $Ba_{0.6}K_{0.4}Fe_2As_2$ samples prepared from hydrides revealed high crystallinity of the product and absence of significant Ba/K clustering, thus confirming the appropriatness of hydride route for the preparation of $Ba_{1-x}K_xFe_2As_2$ superconductors. Local ordering along [110] crystallographic direction can be an intrinsic property or a kinetically induced phenomenon. More

dx.doi.org/10.1021/ja509907r | J. Am. Chem. Soc. 2014, 136, 16932–16939

studies are currently underway, including high-temperature calorimetric investigations.

DISCUSSION

Several methods of preparation of $Ba_{1-x}K_xFe_2As_2$ in powdered bulk or in the form of single crystals are reported due to date.[15] Single crystals can be grown from FeAs flux, or KAs-flux (for K-rich compositions), or Sn-flux. The latter is less preferable, since tin inclusions into the crystal structure of $Ba_{1-x}K_xFe_2As_2$ affect its properties. While flux methods give access to large crystals suitable for property measurement, these methods are not suitable for the production of bulk samples or wires.

The classical solid-state method to produce bulk materials involves combining elemental Ba, K, Fe, As and heating them in inert atmosphere. This method requires multiple annealing, pressing of the pellets, and regrinding in order to achieve a homogeneous distribution of reactants and improve slow kinetics. In some cases, to minimize the loss of potassium by evaporation, the volume of the alumina crucibles is reduced by alumina inlays. All these precautions are needed owing to the drastically different reactivity of the starting reagents: volatile As (sublimes at 887 K), low-melting and volatile K (mp 336 K; bp 1032 K), and quite inert Fe (mp 1811 K). The reaction Ba + K + Fe + As → $Ba_{1-x}K_xFe_2As_2$ proceeds through the solid state, and homogeneous mixing of all the starting materials is important. Given the nature of potassium as a soft sticky metal, the mixing of the elemental Ba, K, Fe, As can be an issue. To overcome this difficulty, binary arsenides, KAs, BaAs, and Fe_2As have been suggested as precursors,[16] however the precursors are not commercially available and need to be synthesized. Salt-like barium and potassium hydrides are suitable precursors for the synthesis of $Ba_{1-x}K_xFe_2As_2$ since they provide better mixing of the components. After decomposition of KH (~673 K), the resulting potassium is already intimately mixed with Fe/As, thus leading to faster formation of the target phase. According to PXRD and magnetic data, $Ba_{1-x}K_xFe_2As_2$ prepared from hydrides has the same structural and superconducting properties as $Ba_{1-x}K_xFe_2As_2$ obtained from elements. The hydride route is being suggested for the preparation of the superconducting $Ba_{1-x}K_xFe_2As_2$ wires by the *in situ* PIT method owing to its simplicity and fast kinetics. This method can be also extended to other iron arsenide superconductors, such as $BaFe_{2-x}Co_xAs_2$, where slow kinetics is known to be an issue, as well as to other arsenides, such as NaFeAs and LiFeAs, and even superconducting selenides, such as KFe_2Se_2.

CONCLUSION

We have developed an efficient and easy method for the preparation of superconducting $Ba_{1-x}K_xFe_2As_2$ from the hydrides BaH_2 and KH. This method is a simple and fast alternative to the traditional solid-state route and includes short ball milling of corresponding hydrides and either FeAs or elemental Fe and As and heat treatment at 973 or 1073 K in sealed Nb containers. The hydride route to $Ba_{1-x}K_xFe_2As_2$ can be explored for the preparation of superconducting $Ba_{1-x}K_xFe_2As_2$ wires by the *in situ* PIT method owing to its simplicity and fast kinetics. This method can be also extended to other iron arsenide superconductors as well as some selenides because of the availability of the corresponding hydrides and versatility of the proposed method.

ASSOCIATED CONTENT

Supporting Information

Tables S1−S2 and Figures S1−S9. This material is available free of charge via the Internet at http://pubs.acs.org.

AUTHOR INFORMATION

Corresponding Authors

smkauzlarich@ucdavis.edu
yzaikina@ucdavis.edu

Notes

The authors declare no competing financial interest.

ACKNOWLEDGMENTS

We thank Peter Klavins (UC Davis) for assistance with the SQUID measurements and Dr. Mike Hayward (Inorganic Chemistry Laboratory at Oxford University) for advice on the pressure relief apparatus. Financial support from the NSF (Grant NSF DMR-1100313) is gratefully acknowledged. J.V.Z. thanks UC Davis for financial support. Use of the Advanced Photon Source at Argonne National Laboratory was supported by the U.S. Department of Energy, Office of Science, Office of Basic Energy Sciences, under contract no. DE-AC02−06CH11357.

REFERENCES

(1) Johnston, D. C. *Adv. Phys.* **2010**, *59*, 803−1061.
(2) Kamihara, Y.; Watanabe, T.; Hirano, M.; Hosono, H. *J. Am. Chem. Soc.* **2008**, *130*, 3296−3297.
(3) Ganguli, A. K.; Prakash, J.; Thakur, G. S. *Chem. Soc. Rev.* **2013**, *42*, 569−598.
(4) Rotter, M.; Tegel, M.; Johrendt, D.; Schellenberg, I.; Hermes, W.; Pottgen, R. *Phys. Rev. B* **2008**, *78*, 020503.
(5) Cortes-Gil, R.; Parker, D. R.; Pitcher, M. J.; Hadermann, J.; Clarke, S. J. *Chem. Mater.* **2010**, *22*, 4304−4311.
(6) Avci, S.; Allred, J. M.; Chmaissem, O.; Chung, D. Y.; Rosenkranz, S.; Schlueter, J. A.; Claus, H.; Daoud-Aladine, A.; Khalyavin, D. D.; Manuel, P.; Llobet, A.; Suchomel, M. R.; Kanatzidis, M. G.; Osborn, R. *Phys. Rev. B* **2013**, *88*, 094510.
(7) Rotter, M.; Pangerl, M.; Tegel, M.; Johrendt, D. *Angew. Chem., Int. Ed.* **2008**, *47*, 7949−7952.
(8) Bukowski, Z.; Weyeneth, S.; Puzniak, R.; Moll, P.; Katrych, S.; Zhigadlo, N. D.; Karpinski, J.; Keller, H.; Batlogg, B. *Phys. Rev. B* **2009**, *79*, 104521.
(9) Canfield, P. C.; Bud'ko, S. L. *Annu. Rev. Condens. Matter Phys.* **2010**, *1*, 27−50.
(10) Jiang, S.; Xing, H.; Xuan, G. F.; Wang, C.; Ren, Z.; Feng, C. M.; Dai, J. H.; Xu, Z. A.; Cao, G. H. *J. Phys.: Condens. Matter* **2009**, *21*, 382203.
(11) Rotter, M.; Tegel, M.; Johrendt, D. *Phys. Rev. Lett.* **2008**, *101*, 107006.
(12) Katase, T.; Ishimaru, Y.; Tsukamoto, A.; Hiramatsu, H.; Kamiya, T.; Tanabe, K.; Hosono, H. *Nat. Commun.* **2011**, *2*, 6.
(13) Weiss, J. D.; Tarantini, C.; Jiang, J.; Kametani, F.; Polyanskii, A. A.; Larbalestier, D. C.; Hellstrom, E. E. *Nat. Mater.* **2012**, *11*, 682−685.
(14) Ma, Y. W. *Supercond. Sci. Technol.* **2012**, *25*, 113001.
(15) Sefat, A. S. *Curr. Opin. Solid State Mater. Sci.* **2013**, *17*, 59−64.
(16) Avci, S.; Chmaissem, O.; Chung, D. Y.; Rosenkranz, S.; Goremychkin, E. A.; Castellan, J. P.; Todorov, I. S.; Schlueter, J. A.; Claus, H.; Daoud-Aladine, A.; Khalyavin, D. D.; Kanatzidis, M. G.; Osborn, R. *Phys. Rev. B* **2012**, *85*, 184507.
(17) Ma, X. C.; Xu, F.; Atkins, T. M.; Goforth, A. M.; Neiner, D.; Navrotsky, A.; Kauzlarich, S. M. *Dalton Trans.* **2009**, 10250−10255.
(18) Yi, T. H.; Chen, S. P.; Li, S.; Yang, H.; Bux, S.; Bian, Z. X.; Katcho, N. A.; Shakouri, A.; Mingo, N.; Fleurial, J. P.; Browning, N. D.; Kauzlarich, S. M. *J. Mater. Chem.* **2012**, *22*, 24805−24813.

(19) Petricek, V.; Dusek, M.; Palatinus, L. *JANA2000: The Crystallographic Computing System*; Institute of Physics: Praha, Czech Republic, 2000.
(20) Berar, J. F.; Lelann, P. *J. Appl. Crystallogr.* **1991**, *24*, 1−5.
(21) Rozsa, S.; Schuster, H. U. *Z. Naturforsch., B: J. Chem. Sci.* **1981**, *36*, 1668−1670.
(22) Rudd, D. W.; Johnson, S.; Vose, D. W. *J. Phys. Chem.* **1962**, *66*, 351−&.
(23) Buxbaum, R. E.; Kinney, A. B. *Ind. Eng. Chem. Res.* **1996**, *35*, 530−537.
(24) Yukawa, H.; Nambu, T.; Matsumoto, Y.; Watanabe, N.; Zhang, G. X.; Morinaga, M. *Mater. Trans.* **2008**, *49*, 2202−2207.
(25) Hosono, H.; Matsuishi, S. *Curr. Opin. Solid State Mater. Sci.* **2013**, *17*, 49−58.
(26) Hanna, T.; Muraba, Y.; Matsuishi, S.; Igawa, N.; Kodama, K.; Shamoto, S.; Hosono, H. *Phys. Rev. B* **2011**, *84*, 7.
(27) Matsuishi, S.; Hanna, T.; Muraba, Y.; Kim, S. W.; Kim, J. E.; Takata, M.; Shamoto, S.; Smith, R. I.; Hosono, H. *Phys. Rev. B* **2012**, *85*, 6.
(28) Terashima, T.; Kimata, M.; Satsukawa, H.; Harada, A.; Hazama, K.; Uji, S.; Harima, H.; Chen, G.-F.; Luo, J.-L.; Wang, N.-L. *J. Phys. Soc. Jpn.* **2009**, *78*, 063702.
(29) Dong, J. K.; Zhou, S. Y.; Guan, T. Y.; Zhang, H.; Dai, Y. F.; Qiu, X.; Wang, X. F.; He, Y.; Chen, X. H.; Li, S. Y. *Phys. Rev. Lett.* **2010**, *104*, 087005.
(30) Sasmal, K.; Lv, B.; Lorenz, B.; Guloy, A. M.; Chen, F.; Xue, Y.-Y.; Chu, C.-W. *Phys. Rev. Lett.* **2008**, *101*, 107007.
(31) Fukazawa, H.; Yamada, Y.; Kondo, K.; Saito, T.; Kohori, Y.; Kuga, K.; Matsumoto, Y.; Nakatsuji, S.; Kito, H.; Shirage, P. M.; Kihou, K.; Takeshita, N.; Lee, C. H.; Iyo, A.; Eisaki, H. *J. Phys. Soc. Jpn.* **2009**, *78*, 083712.
(32) Rotter, M.; Tegel, M.; Schellenberg, I.; Schappacher, F. M.; Pottgen, R.; Deisenhofer, J.; Gunther, A.; Schrettle, F.; Loidl, A.; Johrendt, D. *New J. Phys.* **2009**, *11*, 025014.
(33) Park, J. T.; Inosov, D. S.; Niedermayer, C.; Sun, G. L.; Haug, D.; Christensen, N. B.; Dinnebier, R.; Boris, A. V.; Drew, A. J.; Schulz, L.; Shapoval, T.; Wolff, U.; Neu, V.; Yang, X. P.; Lin, C. T.; Keimer, B.; Hinkov, V. *Phys. Rev. Lett.* **2009**, *102*, 117006.
(34) Song, C.-L.; Yin, Y.; Zech, M.; Williams, T.; Yee, M. M.; Chen, G.-F.; Luo, J.-L.; Wang, N.-L.; Hudson, E. W.; Hoffman, J. E. *Phys. Rev. B* **2013**, *87*, 214519.
(35) Fukazawa, H.; Yamazaki, T.; Kondo, K.; Kohori, Y.; Takeshita, N.; Shirage, P. M.; Kihou, K.; Miyazawa, K.; Kito, H.; Eisaki, H.; Iyo, A. *J. Phys. Soc. Jpn.* **2009**, *78*, 033704.
(36) Goko, T.; Aczel, A. A.; Baggio-Saitovitch, E.; Bud'ko, S. L.; Canfield, P. C.; Carlo, J. P.; Chen, G. F.; Dai, P. C.; Hamann, A. C.; Hu, W. Z.; Kageyama, H.; Luke, G. M.; Luo, J. L.; Nachumi, B.; Ni, N.; Reznik, D.; Sanchez-Candela, D. R.; Savici, A. T.; Sikes, K. J.; Wang, N. L.; Wiebe, C. R.; Williams, T. J.; Yamamoto, T.; Yu, W.; Uemura, Y. J. *Phys. Rev. B* **2009**, *80*, 6.
(37) Yeoh, W. K.; Gault, B.; Cui, X. Y.; Zhu, C.; Moody, M. P.; Li, L.; Zheng, R. K.; Li, W. X.; Wang, X. L.; Dou, S. X.; Sun, G. L.; Lin, C. T.; Ringer, S. P. *Phys. Rev. Lett.* **2011**, *106*, 247002.